The Effect of Anisotropy on the Potential Distribution in Biological Tissue and its Impact on Nerve Excitation Simulations

Robert B. Szlavik, *Member, IEEE*, and Hubert de Bruin*, *Member, IEEE*

***Abstract*—We present a finite difference solution of the potential distribution associated with electrical current stimulation in an anisotropic in-homogeneous tissue environment and compare it to the isotropic case. The results demonstrate that there can be significant errors associated with the assumption of isotropic tissue properties in calculating the potential distribution along an axon in nerve excitation simulations. These errors can have a significant impact on predicted nerve fiber recruitment patterns when evaluating the efficacy of specific surface or intramuscular stimulus electrode configurations. The results of this study also suggest when a more comprehensive tissue model should be implemented in an electrode design study. Simulation results indicate that the isotropy assumption is worst under bipolar electrode stimulation as opposed to monopolar stimulation and that the bipolar error increases as the distance between electrodes decreases. In light of these results, it is concluded that in order to avoid large errors in the calculated potential distribution along an axon, the isotropy assumption should only be used when the transverse depth from the electrode to the nerve is relatively small.**

***Index Terms*—Nerve stimulation, tissue anisotropy, volume conductor fields.**

I. Introduction

MOTOR nerves are routinely stimulated in electrodiagnostics to determine the conduction velocities of individual fibers and populations of fibers, or to estimate the number of motor units in a selected muscle [1]–[3]. Both surface [2] and intramuscular [1], [3] electrodes are used to stimulate the nerve fibers as well as a range of stimulus pulse durations. Functional electrical stimulation (FES) also employs a wide variety of electrode configurations and stimulation protocols. In our research, we would like to determine what effect electrode configuration or stimulus waveform has on the selective stimulation of populations of nerve fibers with different diameters. To gain a theoretical understanding of these effects and guide the design of in vivo experiments, simulation studies can be performed using sufficiently accurate models of nerve fiber populations and the surrounding biological tissues. This paper presents the results of including tissue anisotropy in such simulation studies.

Manuscript received August 9, 1999; revised April 25, 2000. This research was supported by a grant from the Natural Sciences and Engineering Research Council of Canada (NSERC). *Asterisk indicates corresponding author.*

R. B. Szlavik is with the Department of Electrical and Computer Engineering, McMaster University, Hamilton, ON, L8S 1Z5, Canada (e-mail: rszlavik@on.aibn.com)

*H. de Bruin is with the Departments of Electrical and Computer Engineering and Medicine, McMaster University, Hamilton, ON, L8S 1Z5 , Canada (e-mail: debruin@mcmaster.ca).

Publisher Item Identifier S 0018-9294(00)08003-4.

The approach that has been adopted by several investigators is to assume that the surrounding tissue in the nerve excitation simulations is isotropic, homogeneous and infinite or semi-infinite [4]–[7]. These assumptions lead to a simple closed form expression for the potential that can be derived from the elemental form of Ohms Law

$$V(x, y) = \frac{I_{ext}\rho}{4\pi\sqrt{(x - x_o)^2 + (y - y_o)^2}}. \tag{1}$$

Although in general the relationship in (1) can be extended to three dimensions, a two-dimensional (2-D) potential profile can be generated where I_{ext} is the magnitude of the injected current and ρ is the tissue resistivity. The variables x and y represent the longitudinal and transverse distance from the monopolar current electrode that is located at x_o and y_o. Implicit in the form of (1) is that the point current source lies in the same plane as the axon.

The fact that tissue can be anisotropic has been known for some time [8]–[10]. Some of the earlier papers that reported anisotropic tissue conductivity focused on pulse measurements [9]. More recently, investigators have made broad spectrum measurements of anisotropic conductivity using swept sinusoidal excitation current sources as well as current pulse transient techniques [11], [12]. It has been demonstrated that considerable variation exists in the tissue conductivity, as a function of excitation frequency [11]. The conductivity anisotropy in tissue such as skeletal muscle has been documented experimentally and theoretical models have been proposed based on a simplified structural geometry of the muscle fibers and their electrical properties [13].

There have been many volume conduction models presented in the literature that have accounted for the anisotropy associated with different tissue structures. Plonsey demonstrated a coordinate transformation technique that is useful for modeling anisotropy in idealized volume conductors [14]. Altman went further by investigating nerve fiber threshold current requirements in an idealized, infinite homogeneous and isotropic volume conductor given an anisotropic nerve fascicle [15]. Veltink and his colleagues used anisotropic volume conduction models to study extraneural and intrafascicular electrode recruitment characteristics [16], [17]. Struijk *et al.*have also used anisotropic volume conduction models to study spinal cord stimulation mechanisms [18].

From a computation perspective, there are many options to choose from when calculating the potential distribution in a volume conductor. In the case of symmetric geometries with idealized inhomogeneous structures, some investigators have

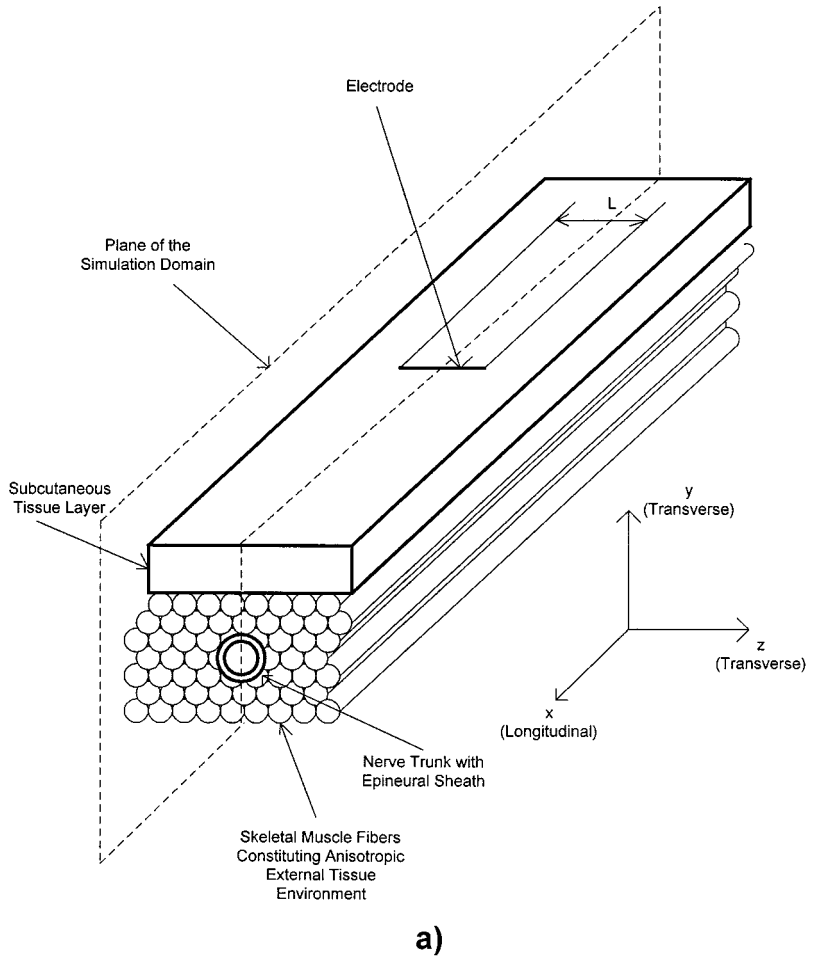

Fig. 1. Representation of a section of tissue. (a) The section shown in (a) includes a 5-mm layer of isotropic subcutaneous tissue. The electrode is assumed to lie on the surface of the subcutaneous tissue layer and the return electrode is assumed to be at infinity for the monopolar case. The plane passes through the idealized nerve trunk structure that consists of a 1-mm-thick isotropic epineurium with a 2-mm inner diameter that surrounds a single anisotropic nerve fascicle. The depth of the nerve trunk from the surface of the subcutaneous tissue layer is 10 mm.

opted to develop closed form solutions [17]. In situations with more complicated geometries, various numerical techniques, such as the finite difference approach, have proved useful [16], [18].

We have investigated the effect of the isotropy assumption by undertaking finite difference simulations of the potential profiles that result from point source surface stimulation, using different electrode configurations, in an anisotropic and inhomogeneous tissue environment. These profiles were compared to those derived for a purely isotropic exterior tissue environment, where the parallel and transverse conductivities from the anisotropic case have been averaged. These simulations can be easily extended to point source intramuscular stimulation. A nerve fiber recruitment study, using different stimulus electrode configurations and a representative population of motor nerve fibers, was also performed to evaluate the impact of the isotropy assumption.

II. Method

A. Calculation of Potential Fields

The finite difference technique lends itself well to electromagnetic field problems in which there are inherent anisotropies associated with the electrical properties of the material under investigation. In addition, the technique can be readily applied where there are inhomogeneities that would make a closed form solution impractical [19].

The finite difference simulations undertaken in this study involved a 2-D resistive grid where it was assumed that the field quantities do not vary in the third dimension. Fig. 1 illustrates the highly idealized geometry associated with the simulations. The nerve trunk has been simplified to a single fascicle with epineurium which is collinear and lies within muscle fibers. This would be a very simplified representation of the motor nerves in a human limb where these nerves lie deep between different muscles. Perineural and endoneural tissues have been ignored. As well, the diameter for the fascicle is slightly larger than would be encountered in man to allow the calculation of intraneural fields using the grid spacing selected. The electrodes are approximated as point current sources that lie on the surface of an isotropic subcutaneous tissue layer. For the sake of simplicity, the effect of skin impedance has been ignored because of high resistivity [20]. A condition of zero current flow normal to the boundary was instituted for the tissue surface with the exception of electrode nodes. These constraints constitute the Neumann boundary condition at the tissue surface. Inside the

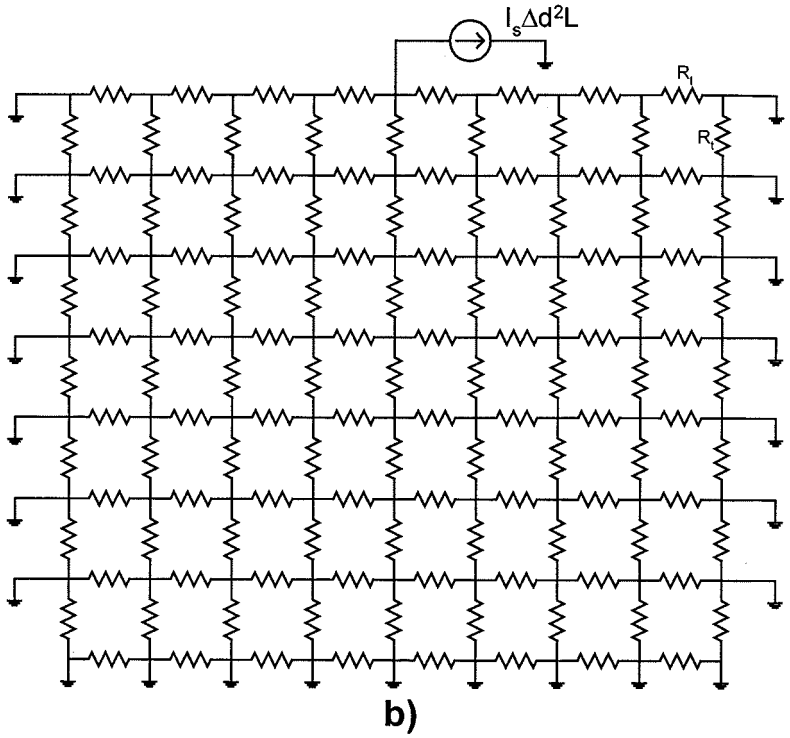

Fig. 1. (*Continued*.) Representation of a section of tissue. The circuit shown in (b) illustrates the finite difference simulation mesh with $\boldsymbol{R_l}$ and $\boldsymbol{R_t}$ representing the longitudinal and transverse resistances taken from the plane of the simulation domain for the tissue sample. The grid used in the simulation consists of 253 × 252 nodes with node spacing $\Delta \boldsymbol{d}$. In a 2-D representation the current source I_S becomes a point source as shown, scaled by $L = 10$ mm which is the length of the electrodes in the z direction. A stimulus current amplitude of 100 mA was used in these simulations.

tissue, at relatively large longitudinal and transverse distances from the electrode, the potential would decay to zero. A zero-potential Dirichlet boundary condition was, therefore, applied to the other three simulation boundaries. Truncation of the simulation domain at points where the potential is relatively constant is permitted [19]. When using the field simulations in conjunction with nerve excitation studies, the validity of the finite domain size approximation is reinforced since the spatial distribution of the excitation currents driving the nerve fiber is proportional to the second derivative of the extracellular potential along the length of the fiber [21]. This application can be used as a further check of the adequacy of the simulation domain size.

The formulation of the finite difference equations follow from three fundamental relationships of electromagnetic theory, specifically the divergence of the current density, the elemental form of Ohm's Law, and the equivalence between the electric field and the negative gradient of the scalar potential

$$\nabla \cdot J = I_s \tag{2}$$

$$J = \sigma E \tag{3}$$

$$E = -\nabla \phi. \tag{4}$$

In (2)–(4), $\boldsymbol{J}$ represents the current density in A/m^2, $\boldsymbol{I_s}$ is the source current density in A/m^3, σ is the conductivity tensor in S/m, ϕ is the potential in volts and $\boldsymbol{E}$ represents the electric field in V/m. These expressions can be combined resulting in

$$\nabla \cdot (\sigma(-\nabla \phi)) = I_s. \tag{5}$$

The above equation can be written in terms of the discrete voltages defined at the points of the simulation domain grid. In two dimensions, the discrete form of (5) can be written as

$$[\sigma_l(V_2 - V_0) + \sigma_l(V_1 - V_0) + \sigma_t(V_3 - V_0) + \sigma_t(V_4 - V_0)]L = \begin{cases} I_s \Delta d^2 L & (x_0, y_0) = (x_s, y_s) \\ 0 & (x_0, y_0) \neq (x_s, y_s) \end{cases}. \tag{6}$$

In (6) σ_l and σ_t represent the longitudinal and transverse conductivities in the tissue external to the nerve trunk and within the nerve fascicle. The voltages $\boldsymbol{V}_0$, $\boldsymbol{V}_1$, $\boldsymbol{V}_2$, $\boldsymbol{V}_3$, and $\boldsymbol{V}_4$ represent the potentials associated with a computational cell as shown in Fig. 2 [22]. Since the longitudinal and transverse spacings between the mesh nodes were chosen to be equal, the spacing is symbolically represented by $\Delta \boldsymbol{d}$. The field quantities in the z direction, as per Fig. 1, are assumed to be uniform everywhere under the electrode in the z dimension. This simulation does not account for fringing effects associated with the boundaries of the electrode length. These should have a minimal impact on nerve excitation studies since it is assumed that the nerve is located under the middle of the electrodes in the z direction. It should be noted that the right hand side of (6) is zero everywhere in the computational domain except node $(\boldsymbol{x_s}, \boldsymbol{y_s})$ where the source current electrode is attached.

All anisotropic simulations in this study assumed a transverse resistivity of 6.75 Ωm and a longitudinal resistivity of 2.4 Ωm for the tissue medium external to the nerve trunk. These resistivity values were chosen to be consistent with skeletal muscle tissue [11]. The resistivity values associated with the nerve fascicle for the transverse and longitudinal directions were 12.5 and

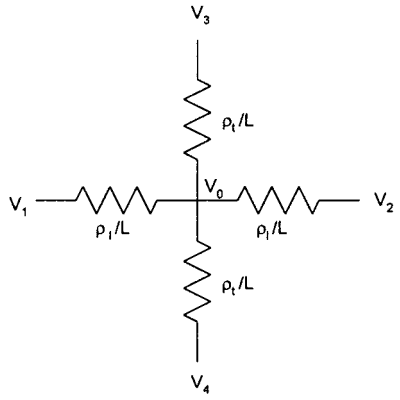

Fig. 2. Diagram of the computational cell associated with the finite difference simulations implemented in this study where ρ_l and ρ_t are the longitudinal and transverse resistivities, respectively, V_1 through V_4 are the potentials relative to V_0 as per (6) and L is the length along the electrode in the z direction.

2.0 Ωm, respectively. The epineurium resistivity was 10 Ωm and the subcutaneous tissue layer resistivity was 25.0 Ωm [16]. Electrical properties of the nerve trunk were assumed to be the same for both the anisotropic and isotropic field calculations. For the isotropic simulations, the external tissue transverse and longitudinal resistivities were averaged to give a resistivity of 4.575 Ωm.

We chose a spacing of $\Delta \boldsymbol{d} = 0.5$ mm between the mesh node points. When using the finite difference field simulations in conjunction with nerve excitation studies, the choice of the mesh spacing becomes an issue. Unlike a closed form potential solution as per (1), where the potential is defined everywhere, the finite difference solution only defines the potential at the mesh nodes. The spacing of Nodes of Ranvier in peripheral nerve fibers is dependent on the size of the fiber as typified by the often quoted relationship [23] between the Nodes of Ranvier spacing and the fiber diameter

$$\frac{K}{D} = 100. \tag{7}$$

In peripheral motor nerves, the fibers range in diameter between approximately 1–18 μm which corresponds to a spacing between the Nodes of Ranvier of 100 μm and 1.8 mm, respectively [24], [25]. Since ultimately, the potential at the Nodes of Ranvier for different size fibers will have to be interpolated from the values calculated at the finite difference mesh points, it is reasonable to choose a value for the mesh spacing that is in this range and is a compromise between spatial resolution and the computational effort required to represent a relatively large tissue volume by a large number of nodes.

For a 253 by 252 node simulation domain, which equates to a cross-sectional area of 126 × 125.5 mm, the solution of the linear system of equations generated by (6) at the mesh nodes is best undertaken using an iterative Gauss Seidel approach. It is advantageous to accelerate the rate of convergence of the solution by modifying the iterative technique to incorporate successive over relaxation [19]. In our study, a relaxation constant of 1.9 was used. Each finite difference simulation was iterated until the change in the potential of each node was less than 100 μV.

It is advisable, in terms of storage considerations, to take advantage of the sparse nature of the admittance matrix. In our experience, solution of systems of equations of the size we have presented here by matrix inversion techniques is not advisable since this approach, in its most basic form, necessitates storage of the entire admittance matrix in its full form and precludes taking advantage of its inherent sparseness.

B. Nerve Fiber Recruitment Study

Nerve fiber excitation simulations have received a great deal of attention in the literature over the last several years where the focus has often been on the nerve fiber equivalent circuit models. A study was designed to test whether the potential differences resulting from tissue anisotropy were significant enough to alter the pattern of recruitment of nerve fibers.

We randomly generated a sample population of axons consistent with the distribution of efferent fiber sizes found in peripheral motor nerves with average diameter 9.53 μm and range from 2 to 18 μm [24], [25] as shown in Fig. 4. The fiber diameters were randomly assigned into five groups of ten and located at different depths within the nerve fascicle in the potential field simulation domain. We used a simplified myelinated axon equivalent circuit model composed purely of linear conductances similar to the axon model used by Sweeney *et al.* [26] and shown here in Fig. 3. The appropriate equivalent circuit conductance parameters, based on the fiber size, were calculated for each nerve fiber in the population.

The field simulation data were used to obtain a vector of potentials along the length of each fiber. The potential values were then interpolated to obtain a profile of potentials at the nodes of Ranvier along each nerve fiber, which were then used to calculate the change in each fiber's transmembrane potential. If the change in the transmembrane potential anywhere along the nerve fiber exceeded a fixed value of 25 mV, the axon was assumed to have fired. The simulation was carried out for each electrode configuration for the anisotropic and isotropic tissue cases. In both cases, the same population of randomly generated nerve fiber sizes was used.

III. Results

A. Effect of Anisotropy on Potential Fields in Tissue

The principal goal of this study was to quantitatively compare the difference in potential solutions in tissue under the assumptions of anisotropy and isotropy for different electrode configurations and geometries. The absolute relative errors resulting from the assumption of isotropy of the tissue external to the nerve trunk were calculated using

$$V_d = \frac{|V_a(x) - V_i(x)|}{\max[|V_a(x)|]} * 100 \qquad (\%). \tag{8}$$

In this normalized difference expression, $\boldsymbol{V_d}$ represents the relative difference in potential between the anisotropic and isotropic cases as a function of the longitudinal distance from the middle of the simulation domain represented by x. The variables $\boldsymbol{V_a}$ and $\boldsymbol{V_i}$ represent the anisotropic and isotropic potentials, respectively, as functions of x, and the normalizing factor is the maximum anisotropic field calculated for each depth.

Fig. 5 is a plot of $\boldsymbol{V_d}$ at different transverse tissue depths for a monopolar stimulating electrode configuration. In gen-

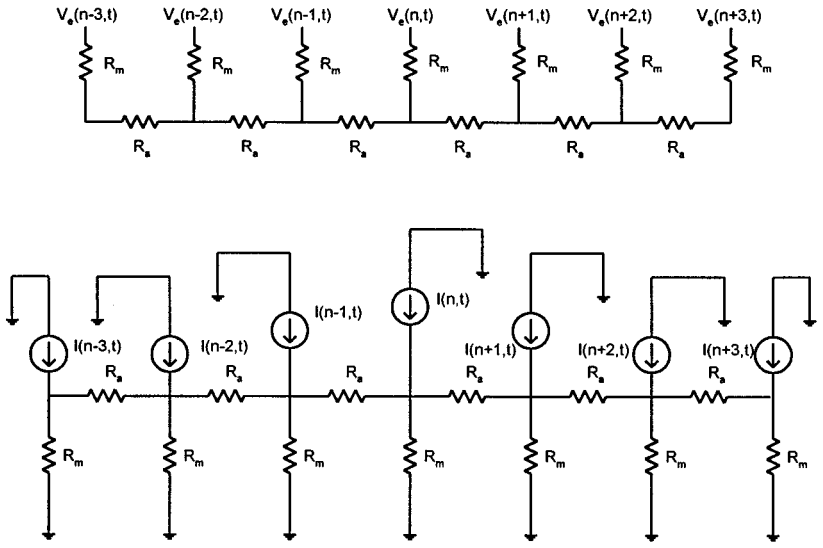

Fig. 3. Equivalent circuit models of a myelinated nerve fiber. The top circuit explicitly shows the external voltage along the fiber as individual sources $V_e(n, t)$. In the second circuit, the sources have been transformed to internally injected currents $I(n, t)$. The membrane resistance R_m and the axoplasmic resistance R_a remain the same for both circuits. The parameters of interest are shown in Table I.

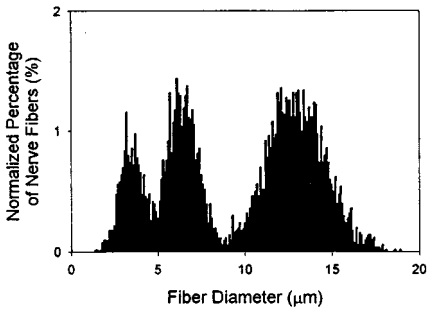

Fig. 4. Sample distribution of 5000 randomly generated nerve fibers. The probability density function used to generate the distribution illustrated is identical to the one used to generate the 50 fibers used in the nerve fiber excitation simulations.

TABLE I
SUMMARY OF THE PARAMETER VALUES AND FORMULAS USED TO CALCULATE THE VALUES OF THE EQUIVALENT CIRCUIT COMPONENTS SHOWN IN FIG. 3. THE FIBER RADIUS IS ASSUMED TO CONSIST OF THE AXON RADIUS AND THE THICKNESS OF THE MYELIN SHEATH. ONLY THE UNITS ARE INDICATED FOR THE FIBER AND AXON DIAMETERS AND RADII SINCE THESE VALUES ARE GENERATED IN THE SIMULATION

ρ_a	Axoplasm Resistivity	1.1 (Ωm)
g_m	Membrane Conductance	304 (S/m^2)
l	Node of Ranvier Width	2.5 (μm)
D	Fiber Diameter	(m)
d	Axon Diameter	(m)
A	Fiber Radius	(m)
a	Axon Radius	(m)
a/A	Ratio of Axon to Fiber Radius	0.7
K	Nodes of Ranvier Spacing	100×D (m)
R_a	Equivalent Axoplasm Resistance	$(\rho_a K)/(\pi a^2)$ (Ω)
R_m	Equivalent Membrane Resistance	$(2\pi g_m a l)^{-1}$ (Ω)

eral the anisotropic field is less than the isotropic especially directly under the electrode. The relative difference is minimal for short transverse depths in the tissue under the electrode and increases from a maximum of approximately 2% at the electrode to a maximum of approximately 42% at a transverse depth of 20 mm. As expected, the normalized difference falls off with increasing horizontal distance, because of the rapidly decreasing anisotropic and isotropic fields at greater distances from the electrode. It should be noted that from 0–4 mm depth, the normalized difference increases slowly reflecting the smaller field differences in the isotropic subcutaneous layer. From 5–10 mm the differences increase more quickly due to the anisotropic muscle layer, while the small decrease from 11–14 mm reflects the anisotropic nerve trunk common to both simulations.

Simulations were also undertaken to investigate the error associated with bipolar electrode configurations. Bipolar electrode stimulation is commonly used in clinical nerve conduction or other studies where the axis of the electrode dipole is placed parallel to the nerve under test. The same amount of current is injected through one of the electrodes as is removed through the other.

Fig. 6 illustrates the relative potential difference profiles calculated using (8), between the anisotropic and isotropic tissue conductivity cases for bipolar stimulation where the electrodes have been positioned 20 mm apart. Once again, the anisotropic potential fields are generally less than for the purely isotropic simulations and the minimum relative difference in potential is seen for small transverse depths in the tissue. As for the monopolar case, the general trend of increasing relative potential difference is observed with increasing transverse depths from the stimulating electrodes. Overall, the relative error observed in the 20-mm bipolar electrode case is worse than in the monopolar case for regions that are deeper than the subcutaneous tissue layer (5 mm) with a relative potential difference that increases from 1% at the electrodes to 76% at a depth of 20 mm from the surface. As in Fig. 5, the maximum relative potential difference does not increase uniformly with

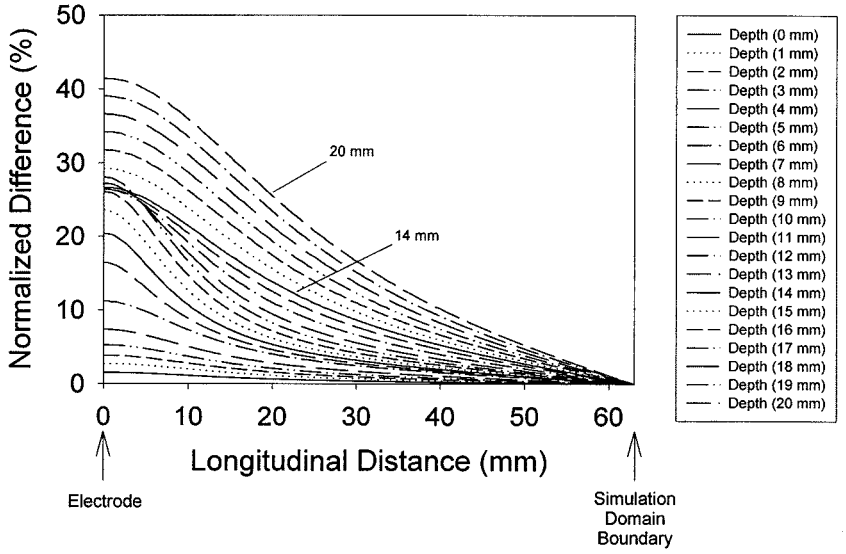

Fig. 5. Relative potential difference profiles between the anisotropic and isotropic tissue simulations with a monopolar electrode configuration. Each curve is the potential difference at a specific depth (distance in the y direction between the point of interest and the surface electrode).

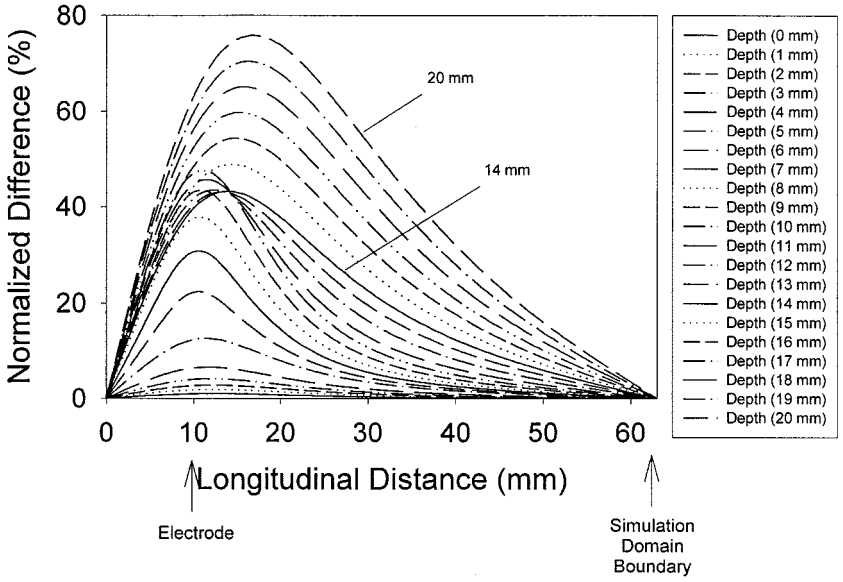

Fig. 6. Relative potential difference profiles between the anisotropic and isotropic tissue simulations with a bipolar electrode spacing of 20 mm. The origin indicates the midpoint between the two electrodes. Each curve is the potential difference at a specific depth or increasing distance in the y direction between the point of interest and the surface electrodes.

increasing depth and a small decrease is observed within the region of the nerve fascicle (10–14 mm).

As the distance between the stimulating electrodes is decreased, there is an increase in the relative difference between the anisotropic and isotropic conductivity cases. The general relative difference trends observed for more closely spaced bipolar electrodes at 10-mm spacing, shown in Fig. 7 are similar to those discussed previously for the 20-mm bipolar and monopolar electrode cases. The more closely spaced electrodes exhibit peak relative potential differences from less than 1% at the electrodes to 78% at a transverse depth of 20 mm from the electrodes.

Fig. 8 summarizes the trends observed in previous figures and shows the maximum difference between the anisotropic and isotropic conductivity cases observed as a function of the transverse depth in the tissue. This graph reinforces the observation that for depths greater than the subcutaneous tissue layer, the overall largest relative potential difference between the isotropic and anisotropic cases is observed in the bipolar electrode case with the smallest electrode separation. The monopolar case exhibits the lowest overall error of the electrode configurations studied. This order is reversed for depths within the subcutaneous tissue layer. The simulation data suggests that for short transverse depths between the point of interest and the electrode, the maximum difference between the anisotropic case and the isotropic case is comparable for all electrode configurations studied. Fig. 8 also demonstrates the decreasing relative errors from 10–14 mm within the region of the nerve trunk.

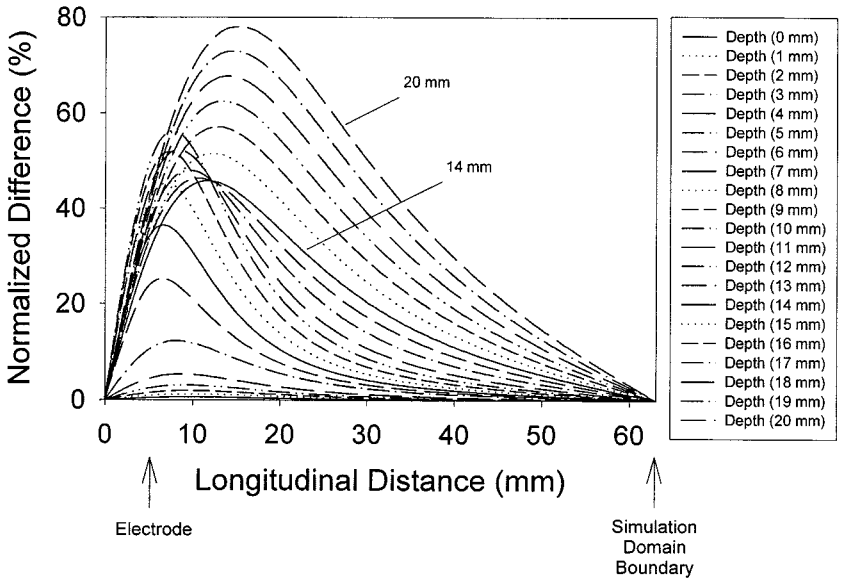

Fig. 7. Relative potential difference profiles between the anisotropic and isotropic tissue simulations with a bipolar electrode spacing of 10 mm. Each curve is the potential difference at a specific depth (transverse distance in the y direction between the point of interest and the surface electrodes).

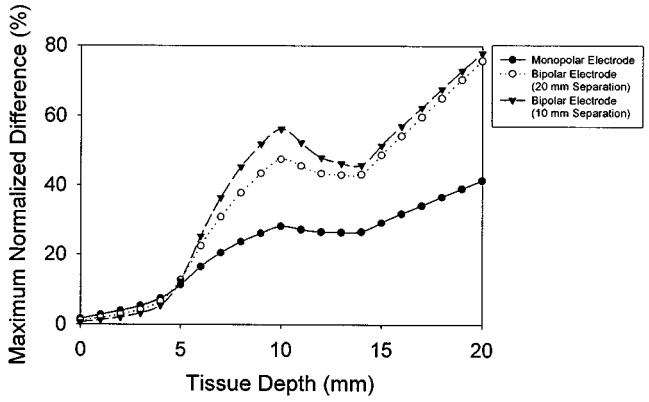

Fig. 8. Maximum relative potential difference profiles as a function of the transverse depth from the surface of the simulated tissue domain for the three electrode configurations.

B. Effect of Anisotropy on Nerve Fiber Recruitment

Fig. 9 consists of a series of histograms that illustrate the difference in recruitment patterns between the anisotropic and isotropic tissue cases for the three different electrode configurations that were studied in these simulations. These histograms illustrate a pattern of decrease in the absolute number of fibers recruited for the anisotropic cases when compared to their isotropic counterparts. Another observation worth noting is the decrease in the absolute range of maximum to minimum diameter recruited fibers that are consistently observed for the anisotropic simulations.

IV. Discussion

A. Effect of Anisotropy on the Simulated Potential Profiles

As expected, a relatively small maximal relative potential difference was observed between the anisotropic and isotropic potential distributions within the surface subcutaneous tissue layer, because the field is similar within this isotropic region for both cases irrespective of electrode geometry. A significant increase in the observed relative potential difference is demonstrated at greater depths where the differences between the isotropic and the anisotropic cases have greater impact on the field distribution. The simulation results also demonstrated that there was a significant change in calculated relative potential difference between the anisotropic and isotropic potential distributions for different electrode configurations. The monopolar electrode configuration exhibited a much smaller relative difference between the isotropic and anisotropic cases than both bipolar configurations at depths greater than the thickness of the subcutaneous tissue layer. There was a marginal, however not insignificant, increase in the relative difference between the anisotropic and the isotropic cases as the bipolar electrode dipole separation decreases.

A significant perturbation in the potential distribution local to the epineural sheath and the nerve fascicle was observed. This perturbation is due to the differences in the electrical properties of the epineural sheath and the nerve fascicle relative to the tissue external to the nerve trunk. The nerve fascicle tissue exhibits significant electrical anisotropy in the directions longitudinal and transverse to the roughly cylindrical axis of the fibers whereas the epineural sheath is isotropic and consists of connective tissue and fat cells with a higher conductivity than the subcutaneous tissue layer but still significantly lower than the transverse conductivity of the anisotropic tissue external to the nerve trunk. The perineurium was not modeled explicitly in these simulations, however it has been demonstrated that for intrafascicular stimulation, the insulating properties of the perineurium are significant in spatial localization of the stimulus [16]. From the perspective of the relative difference calculations, the nerve fiber structure is identical in both the anisotropic and the isotropic simulations and consequently a relatively small decrease in the maximal relative potential difference is observed for depths associated with the nerve trunk region for all electrode configurations.

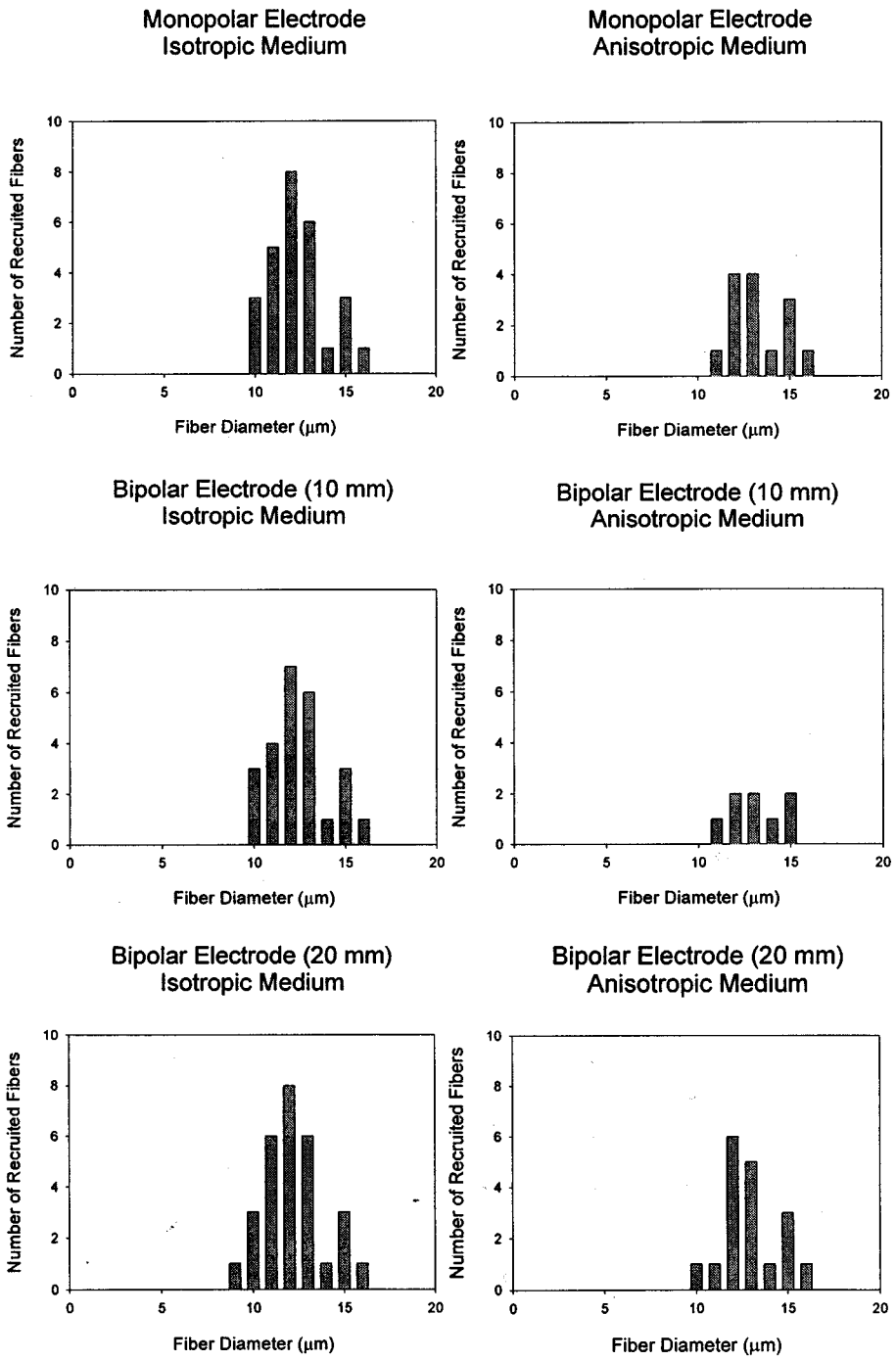

Fig. 9. Histograms illustrating the difference in recruitment patterns between the isotropic and anisotropic tissue domain simulations. The anisotropic histograms consistently illustrate a pattern of fewer recruited nerve fibers than their isotropic counterparts along with a decrease in the absolute range of maximum to minimum fiber diameters recruited.

If an isotropic assumption is made in calculating the resultant potential distribution from an excitation current electrode, then the relative error in the potential is minimal provided that the transverse depth between the point of interest and the electrode is within the depth associated with the subcutaneous tissue layer. As the transverse depth between the electrode and the point of interest is increased, the maximum relative potential difference associated with the isotropic approximation increases. Under anisotropic conditions, a greater drop in the potential in the transverse direction would be expected for the same depth as compared to the isotropic situation, since the current is subjected to a much higher impedance. It is not surprising, therefore, that at greater and greater depths in the tissue, a larger and larger relative difference is observed between the isotropic and the anisotropic potential.

The overall observed relative potential difference is worse for bipolar electrodes with short interelectrode spacing and decreases as the electrode spacing increases for depths in excess of the thickness of the subcutaneous tissue layer. The monopolar electrode, which may be viewed as a limiting case of two bipolar

electrode at an infinite distance apart, exhibits the least overall relative potential difference. As the two bipolar electrodes are placed nearer to each other, there is a greater interaction between the fields generated from the positive current electrode and the negative current electrode. It is not unexpected that the field interaction is different under anisotropic conditions compared to isotropic conditions since more of the current flux would be confined to the regions near the surface of the tissue in the anisotropic case.

B. Effect of Anisotropy on Nerve Fiber Recruitment

The pattern of decrease in number and range of nerve fibers recruited in the anisotropic case is expected since the field simulations showed a decrease in field strength at the nerve trunk depth. The decrease in the range can be principally attributed to some smaller diameter (higher threshold) fibers not being recruited in the anisotropic cases because of the decreased fields at all depths within the nerve. Even some of the larger diameter fibers that are deeper in the simulation domain fail to become recruited as shown in the 10-mm bipolar anisotropic histogram of Fig. 9. Since the decrease in potential fields as a result of anisotropy has a greater effect on the recruitment of smaller fibers, there is also an increase in the average recruited nerve fiber diameter between the isotropic and anisotropic tissue simulations for all three electrode configurations studied.

These results show that greater stimulus currents are required to recruit populations of nerve fibers in nerve trunks situated in anisotropic media. Our simulations considered only anisotropy parallel and transverse to the nerve fiber direction with highest conductivity in the parallel direction. A relatively low conductivity in the transverse and parallel directions would have different results, since there would be lower conductivities both along the nerve fiber and deeper into the tissue. Anisotropy directions not orthogonal to the nerve fibers would give intermediate results. General solutions were beyond the scope of this paper.

REFERENCES

[1] F. C. Want and P. J. Delwaide, "Number and relative size of thenar motor units estimated by an adapted multiple point stimulation method," *Muscle & Nerve*, vol. 18, pp. 969–979, 1995.

[2] V. Galea, H. de Bruin, R. Cavasin, and A. J. McComas, "The numbers and relative sizes of motor units estimated by computer," *Muscle & Nerve*, vol. 14, pp. 1123–1130, Nov. 1991.

[3] R. B. Stein and J. F. Yang, "Methods for estimating the number of motor units in human muscle," *Ann. Neurol.*, vol. 28, pp. 487–495, 1990.

[4] E. N. Warman, W. M. Grill, and D. Durand, "Modeling the effects of electric fields on nerve fibers: Determination of excitation thresholds," *IEEE Trans. Biomed. Eng.*, vol. 39, pp. 1244–1254, Dec. 1992.

[5] F. Rattay, "Modeling the excitation of fibers under surface electrodes," *IEEE Trans. Biomed. Eng.*, vol. 35, pp. 199–202, Mar. 1988.

[6] ——, "Analysis of models for external stimulation of axons," *IEEE Trans. Biomed. Eng.*, vol. BME-33, pp. 974–977, Oct. 1986.

[7] P. N. Robillard and D. Poussart, "Spatial resolution of four electrode array," *IEEE Trans. Biomed. Eng.*, vol. BME-26, pp. 465–470, Aug. 1979.

[8] P. W. Nicholson, "Experimental models for current conduction in an anisotropic medium," *IEEE Trans. Biomed. Eng.*, vol. BME-14, pp. 55–56, Jan. 1967.

[9] S. Rush, J. A. Abildskov, and R. McFee, "Resistivity of body tissues at low frequencies," *Circ. Res.*, vol. 12, pp. 40–50, Jan. 1963.

[10] S. Rush, "Methods of measuring the resistivities of anisotropic conducting media *in situ*," *J. Res. National Bureau of Standards—C, Eng. Instrum.*, vol. 66C, pp. 217–222, July 1962.

[11] F. L. H. Gielen, W. Wallinga-de Jonge, and K. L. Boon, "Electrical conductivity of skeletal muscle tissue: Experimental results from different muscles in vivo," *Med. Biol. Eng. Comput.*, vol. 22, pp. 569–577, 1984.

[12] R. B. Szlavik and H. de Bruin, "Pulsed transient tissue conductivity measurement," in *Proc. 18th Annu. Conf. IEEE-EMBS*, Amsterdam, The Netherlands, 1996, Available: CD-ROM, ISBN 90–9010005–9.

[13] F. L. H. Gielen, H. E. P. Cruts, B. A. Albers, K. L. Boon, W. Wallinga-de Jonge, and H. B. K. Boom, "Model of electrical conductivity of skeletal muscle based on tissue structure," *Med. Biol. Eng. Comput.*, vol. 24, pp. 34–40, 1986.

[14] R. Plonsey, "The active fiber in a volume conductor," *IEEE Trans. Biomed. Eng.*, vol. BME-21, pp. 371–381, Sept. 1974.

[15] K. W. Altman and R. Plonsey, "Point source nerve bundle stimulation: Effects of fiber diameter and depth on simulated excitation," *IEEE Trans. Biomed. Eng.*, vol. 37, pp. 688–698, July 1990.

[16] P. H. Veltink, B. K. Van Veen, J. J. Struijk, J. Holsheimer, and H. B. K. Boom, "A modeling study of nerve fascicle stimulation," *IEEE Trans. Biomed. Eng.*, vol. 36, pp. 683–692, July 1989.

[17] P. H. Veltink, J. A. van Alste, and H. B. K. Boom, "Simulation of intrafascicular and extraneural nerve stimulation," *IEEE Trans. Biomed. Eng.*, vol. 35, pp. 69–75, Jan. 1988.

[18] J. J. Struijk, J. Holsheimer, and H. B. K. Boom, "Excitation of dorsal root fibers in spinal cord stimulation: A theoretical study," *IEEE Trans. Biomed. Eng.*, vol. 40, pp. 632–639, July 1993.

[19] A. Heringa, D. F. Stegeman, G. J. H. Uijen, and J. P. C. de Weerd, "Solution methods of electrical field problems in physiology," *IEEE Trans. Biomed. Eng.*, vol. BME-29, pp. 34–42, Jan. 1982.

[20] F. Rattay, *Electrical Nerve Stimulation*. New York: Springer-Verlag, 1990.

[21] ——, "Analysis of models for extracellular fiber stimulation," *IEEE Trans. Biomed. Eng.*, vol. 36, pp. 676–682, July 1989.

[22] W. F. Ames, *Numerical Methods for Partial Differential Equations*. Toronto, Canada: Academic, 1992.

[23] D. R. McNeal, "Analysis of a model for excitation of myelinated nerve," *IEEE Trans. Biomed. Eng.*, vol. BME-23, pp. 329–337, July 1976.

[24] I. A. Boyd and M. R. Davey, *Composition of Peripheral Nerves*. Edinburgh, U.K.: E & S Livingstone Ltd., 1968.

[25] R. B. Szlavik and H. de Bruin, "Simulating the distribution of axon size in nerves," in *Proc. 23rd Canadian Medical and Biological Engineering Society Conf.*, Toronto, Canada, 1997, pp. 168–169.

[26] J. D. Sweeney, D. A. Ksienski, and J. T. Mortimer, "A nerve cuff technique for selective excitation of peripheral nerve trunk regions," *IEEE Trans. Biomed. Eng.*, vol. 37, pp. 706–715, July 1990.

Robert B. Szlavik (M'89) was born in Hamilton, ON, Canada. He received the B.Eng. (*summa cum laude*), M.Eng. and Ph.D. degrees in electrical and computer engineering from McMaster University, Hamilton, ON, Canada, in 1991, 1994, and 1999, respectively.

He has served as a Sessional Special Lecturer in the Department of Electrical and Computer Engineering at McMaster University. His current research interests include theoretical modeling of the electrical recruitment properties of excitable tissue, experimental electromyography and biomedical instrumentation.

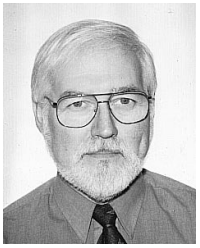

Hubert de Bruin (S'67–M'69) received the B.Eng., M.Eng., and Ph.D. degrees in electrical engineering from McMaster University, Hamilton, ON, Canada, in 1969, 1971, and 1976, respectively.

He was a MRC Fellow in the Department of Medicine, McMaster University from 1976–1979 and joined the Faculty of Health Sciences in 1979. He was also concurrently Director of Biomedical Engineering at Chedoke–McMaster Hospitals from 1984–1995. He is currently Associate Professor in the Departments of Medicine and Electrical and Computer Engineering, McMaster University and Research Coordinator for Rehabilitation at Hamilton Health Sciences Corporation His research interests include diagnostic and kinesiological electromyography and the control of skeletal muscle.